Correlation between magnetism and structural relaxation in thin Fe(001) films patterned by the atomic saw method

H. Jaffrès*
Laboratoire de Physique de la Matière Condensée, UMR 5830, CNRS-UPS-INSA Complexe Scientifique de Rangueil, 31077 Toulouse Cedex 4, France

P. Le Fèvre
Laboratoire pour l'Utilisation du Rayonnement Electromagnétique, Université de Paris–Sud, BP 34, 91898 Orsay Cedex, France

H. Magnan
Laboratoire pour l'Utilisation du Rayonnement Electromagnétique, Université de Paris–Sud, BP 34, 91898 Orsay Cedex, France and Service de Recherche sur les Surfaces et L'Irradiation de la Matière, Commisariat à L'Energie Atomique, 91191 Orsay Cedex, France

A. Midoir and D. Chandesris
Laboratoire pour l'Utilisation du Rayonnement Electromagnétique, Université de Paris–Sud, BP 34, 91898 Orsay Cedex, France

L. Ressier
Laboratoire de Physique de la Matière Condensée, UMR 5830, CNRS-UPS-INSA Complexe Scientifique de Rangueil, 31077 Toulouse Cedex 4, France

A. Schuhl and F. Nguyen Van Dau
Unité mixte de recherches Thomson CSF-CNRS, Laboratoire Central de Recherches, Domaine de Corbeville, 91191 Gif-sur-Yvette, France

M. Goiran, J. P. Peyrade, and A. R. Fert
Laboratoire de Physique de la Matière Condensée, UMR 5830, CNRS-UPS-INSA Complexe Scientifique de Rangueil, 31077 Toulouse Cedex 4, France

(Received 6 August 1999)

We present detailed extended x-ray-absorption fine-structure (EXAFS) studies carried out on 50-Å epitaxial thin films grown by molecular-beam epitaxy on MgO(001) substrate prior and after structuration into ribbons by the so-called ''atomic saw'' method. Because of interfacial strain due to lattice mismatch (+3.8%), the crystallographic structure of the as-deposited film is demonstrated to be body-centered tetragonal with lattice constants $a=2.915\pm0.015$ Å and $c=2.82\pm0.01$ Å. This structure is 2% expanded in plane and −1.6% compressed along the surface normal as compared to the bulk Fe one. After structuration, the patterned 50-Å Fe films show a strong in-plane uniaxial magnetic anisotropy (close to 2.5 kOe). The EXAFS studies provide the clear evidence that the dislocation slipping process enhances a uniaxial relaxation $\delta=-2.5\%$ of the elastic strain field in the Fe film along the direction perpendicular to the ribbons. Through magnetoelastic effects, this relaxation is clearly demonstrated to be at the source of the observed magnetic anisotropy. This paper emphasizes the power of the ''phase derivative'' method in the analysis of EXAFS spectra for the determination of crystalline parameters in the case of bcc-type structures.

I. INTRODUCTION

Epitaxial thin films provide new opportunities to explore the relationship between structure and magnetism. The magnetic properties $3d$ transition-metal thin films are controlled by magnetic anisotropies which are found to be up to several orders of magnitude larger than in bulk materials and reveal the strong influence of the structure at interfaces. Since the discovery of the perpendicular anisotropy in ultrathin ferromagnetic films,[1] the influence on the anisotropy of symmetry breaking at surfaces and interfacial strain due to lattice mismatch have been largely discussed.[2–6] To achieve a better understanding of the nature of the involved anisotropies, some groups have performed experiments on magnetic films grown on stepped surfaces[7–8] or vicinal surfaces like Fe/W(001),[9,10] Co/Cu,[11–15] Co/Pd,[16] Co/Pt(110),[16] and Fe/Ag(001).[17] They have investigated and observed a step-induced in-plane anisotropy favoring a peculiar magnetization direction, either perpendicular or parallel to the surface steps. The origin was often discussed to be magnetoelastic without being clearly and experimentally evidenced. The relationship between magnetism and structure has to be pointed out and a clear explanation of the magnetic behavior requires a precise knowledge of the atomic structure (growth mode, relaxation).

We have recently proposed the so-called ''atomic saw'' (AS) method for generating strong controlled in-plane magnetic anisotropies in thin epitaxial Fe films grown on semi-

conductor substrate.[18,19] We have shown that the uniaxial compression of these systems along the [100]MgO direction could lead to the structuration of the Fe film into submicronic width Fe ribbons characterized by a magnetic easy axis perpendicular to the steps.[20] Magnetoelastic phenomenon was proposed to be at the source of the induced anisotropy without real experimental proofs. Indeed, high-resolution transmission electronic micrography (HRTEM) observations have evidenced the presence of some dislocations located at the Fe/MgO interface that could explain a uniaxial relief of the elastic strain field in this peculiar direction, suggesting the assumption of magnetoelastic effects.[21]

The aim of this work is to show that the strong anisotropy exhibited is connected to a structural anisotropy enhanced by the AS process. Among all methods that are available to accede to the crystalline structure, extended x-ray-absorption fine-structure (EXAFS) is the more suitable in our case. Unlike x-ray diffraction, x-ray-absorption experiments do not require a long-range order which could be partially damaged spoiled by the AS structuration. In addition, the dependence of the absorption spectra on the x-ray polarization direction allows us to probe any structural anisotropy. Last, the ''phase derivative'' (PD) analysis, largely developed here, is very sensitive to slight changes of the crystalline parameters in a bcc-like cell.[22] Consequently, it can lead to a direct measurement of the uniaxial relaxation of the strain field.

The paper is organized as follows. We first describe the sample elaboration and preparation (Sec. II). Then, we present the first structural analysis (Sec. III) and magnetic properties (Sec. IV) induced by the AS structuration. In Sec. V, we present the EXAFS results concerning a 50-Å-thick Fe film before and after the AS process. A clear and detailed description of the ''phase derivative'' (PD) analysis method is also emphasized. The results are discussed in Sec. VI. Our EXAFS results show that the continuous Fe film is 2% expanded in the film plane and -1.6% compressed along the growing axis relative to the bulk value. We show that the AS enhances a -2.5% uniaxial relaxation process along the direction perpendicular to the created steps. Then, the magnetoelastic model is discussed in Sec. VII.

II. SAMPLE PREPARATION

50-Å-thick Fe films were epitaxially grown on a MgO(001) substrate by molecular-beam epitaxy (MBE) at 50 °C in a vacuum of 10^{-10} Torr with a deposition rate of 1–4 Å min^{-1}. During growth, the substrate was rotating in order to avoid to induce any uniaxial anisotropy. Fe epitaxially grows in a bcc-like structure on fcc MgO(001) with the relative orientation: MgO(001) [010]$\|$Fe(001) [110]: the bcc iron lattice is rotated by 45° in the interface plane relative to the MgO fcc structure. The 3.8% lattice mismatch ($a_{\mathrm{Fe,bulk}} = 2.866$ Å and $a_{\mathrm{MgO}} = 4.21$ Å) should also stretch the Fe lattice parallel to the interface. To avoid any oxidation of the Fe film, a 15-Å-thick Pd cap layer was deposited on Fe. Similarly, the fcc Pd ($a_{\mathrm{Pd}} = 3.89$ Å) grows on Fe with a 45° rotation in the interface plane, their relative orientation being Fe(001)[110]$\|$Pd(001)[100]. *In situ* reflection high-energy electron diffraction experiments indicate that both Fe and Pd layers present a smooth growth.[23,24]

The so-called atomic saw (AS) method was developed by Peyrade and co-workers.[18,19] It consists of applying a uniaxial compressive stress on a sample in order to favor the plastic deformation, i.e., the dislocation slipping through the whole system ''substrate and epitaxial film.'' When a dislocation (respectively, n dislocations) crosses the substrate-film interface, it creates a lattice shift equal to one Burger vector b (respectively, $\mathbf{n}\cdot\mathbf{b}$). In theory, if $\mathbf{n}\cdot\mathbf{b}$ is greater than the film thickness, this layer is patterned into separated stripes. First applied to III-V semiconducting structures,[18] this method has been successfully used to cut Fe thin films epitaxially grown on MgO(001) into iron ribbons and dots.[20,25]

The plastic deformation of the whole sample induces dislocation slip throughout the MgO substrate and the thin films along the activated slip systems of the MgO substrate. The activated slip systems of MgO are fixed by choosing the direction of the compression axis. Indeed, plasticity calculations showed that dislocation slip induced by a compression along the [100] direction of MgO is expected to cut the entire Fe film into adjacent ribbons, aligned along the [010] direction of MgO, corresponding to the [110] direction in the Fe film. In practice, samples of 7 mm long by 2 mm large and 0.5 mm thick have been plastically compressed along this compression axis, at room temperature at a constant deformation strain rate of 1 μm/mn, using a Adamel Lhomargy DY26 hard deformation machine. Fe ribbons have been realized using a plastic strain equal to 8%.

III. FIRST STRUCTURAL ANALYSIS

Atomic force microscopy (AFM) observations of the slip line pattern on the surface of the deformed samples have been performed in air, in tapping mode, using the Digital Instruments Nanoscope III. This scanning mode allows a high-resolution topographic imaging of sample surfaces. A statistical analysis of numerous AFM pictures allowed us to evaluate accurately the influence of the plastic strain on the width L of the buried ribbons and their relative vertical shifts Δ.[20] Observations show that the mean values of L and Δ obtained after an 8% plastic strain are, respectively, equal to 100 ± 50 nm and 1 ± 0.5 nm. Cross sections[21,26] of these pictures in the direction perpendicular to the stripes reveal that the angle between the stripe edges and the (001) surface is lower than 10°. If all dislocations slipped in the same (101) or (101) MgO plane, this angle should be equal to 45°. Therefore the structuration is mainly realized by a succession of small steps occurring in neighboring slipping planes with the result that the stepped Fe film can remain continuous even if the total shift is larger than the film thickness.

Cross-sectional observations of the interface Fe film-MgO substrate have been performed by conventional and high-resolution transmission electron microscopy (HRTEM).[21] In some region of the continuous (as-deposited) Fe film, we could observe some ''stand-off'' dislocations located a few nanometers (about 15 Å) away from the Fe-MgO interface. The role of these dislocations is certainly to relax the tensile stress in the volume of the film. First, this confirms that the Fe structure is stretched by the substrate lattice. Furthermore, this study shows that the strain field is relieved from the dislocation position up to the surface. On the other hand, HRTEM observations done on the sample patterned into ribbons reveal the presence of periodic dislocations oriented

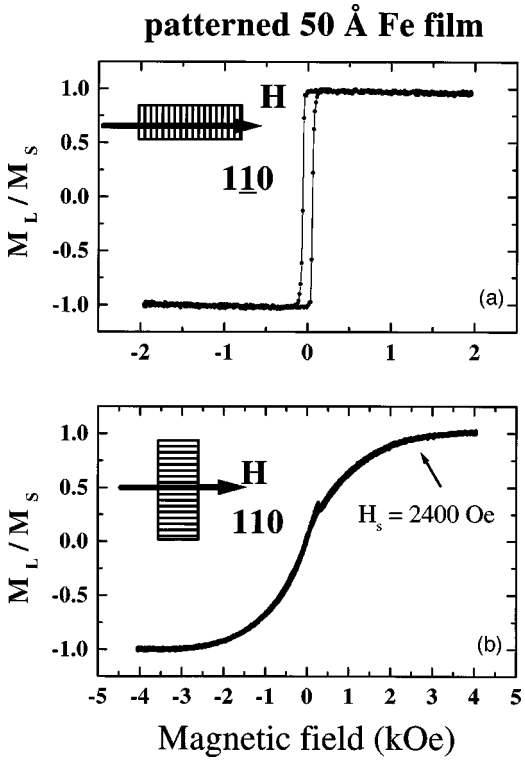

FIG. 1. Magnetization hysteresis cycle measured on the 50-Å patterned Fe film for a magnetic field applied perpendicularly to the ribbons (a) and parallel to the ribbons (b).

parallel to the step edges and located at the interface Fe-MgO. These interface dislocations allow the complete relaxation of the elastic strain field in the Fe layer along the peculiar direction perpendicular to the step edge. Complementary plane view based on Moiré fringes observations have exhibited the uniaxial relaxation of the initial bcc (or tetragonal) cell into a distorted one.[21]

IV. MAGNETIC PROPERTIES

The magnetic properties of the patterned Fe film have been investigated at room temperature by magneto-optical measurements.[20] More detailed discussion about the experimental device are given elsewhere.[27] In order to highlight any anisotropy potentially induced after the atomic saw process, we have studied the magnetization reversal for a magnetic field applied either parallel or perpendicular to the ribbons. Figure 1(a) shows the magnetization reversal measured on the patterned sample for a magnetic field applied perpendicular to the stripes. We can observe a nearly square cycle which is the signature of an abrupt switching of the magnetization from the initial remanent state magnetized perpendicular to the steps to the final one magnetized in the opposite direction. Figure 1(b) displays the magnetization loop recorded for a magnetic field set along the stripe edges. By increasing the magnitude of the field, one can observe that the magnetization gradually rotates from the initial remanent direction perpendicular to the steps towards the direction parallel to the ribbons. The saturation is reached for a relatively high field close to 2400 Oe.[20] This analysis reveals a strong magnetic uniaxial anisotropy (closely dependent on the plastic deformation) which is unexpected from shape energy consideration. In a previous paper, the induced anisotropy was discussed to originate from a magnetoelastic phenomena provoked by a distortion of the initial cubic bcc (or tetragonal) Fe cell into an monoclinic one, as suggested by HRTEM observations.[20] Our hypothesis is that, due to the lattice mismatch between bulk Fe and the MgO substrate, the as-deposited film is in a distorted bcc structure, i.e., stretched in the planes parallel to the interface and therefore compressed along the growth axis. One can thus expect a body-centered tetragonal (bct) structure for the as-deposited thin film characterized by two crystalline parameters a and c [Figs. 2(a) and (b)]. The dislocation slip process should then have for effect to relieve the epitaxial strain along the per-

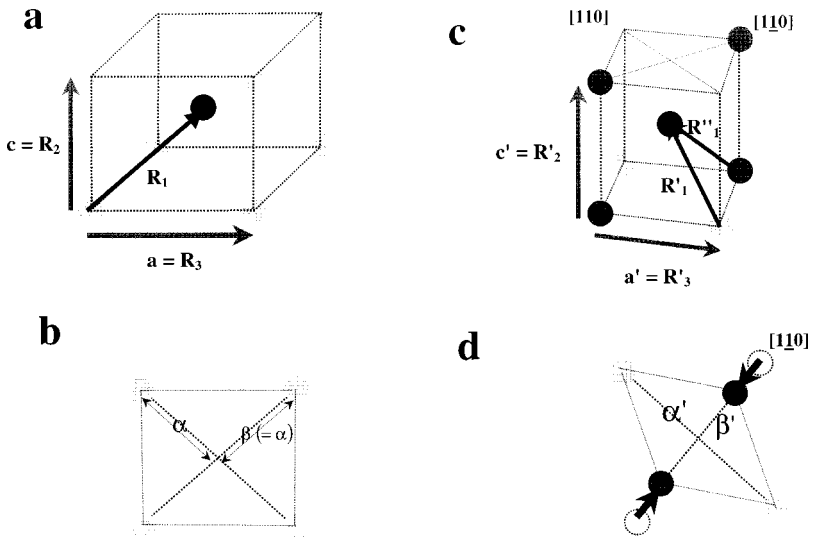

FIG. 2. (a) Body-centered-tetragonal (bct) structure expected in the case of the as-deposited 50-Å Fe thin film. R_1, R_2, and R_3 are the first, second, and third nearest-neighbor distances. (b) (001) In-plane projection of the unit bct cell. α and β stand for the half diagonals of the (001) projection. (c) The bct cell is relaxed along the $[1\bar{1}0]$ direction. R'_1, R''_1, R'_2, and R'_3 are distances between first, second, and third neighbors (structure expected after the atomic saw process). (d) The two half diagonals of the cell's (001) projection are noted α' and β'. The arrows show the relaxation of the cell along the $[1\bar{1}0]$ direction.

pendicular to the ribbons, thus relaxing the bct cell into a monoclinic one. This new structure can be defined by three parameters α', β', and c' [Figs. 2(a) and (b)]. In the next section, we show that experimental evidences can be obtained thanks to EXAFS experiments.

V. EXAFS EXPERIMENTS

A. Introduction

EXAFS (extended x-ray-absorption fine structure) consists in measuring the x-ray-absorption coefficient of the sample as a function of the photon energy. After the Fe *K*-absorption edge, the absorption coefficient shows oscillations (EXAFS), due to the scattering of the photoelectron (created by the photon absorption) wave function by the surrounding neighbors of the excited Fe atom. These oscillations are therefore directly correlated to the structure and the local order around this excited atom.

EXAFS is a very well suited technique for the study of ultrathin epitaxial systems. First, x-ray absorption is element selective: for the samples considered here, spectra recorded at the Fe *K* edge contain only information on the environment of the Fe atoms. Second, taking advantage of the linear polarization of the synchrotron radiation (used as photon source), EXAFS allows us to measure the lattice parameters in all the crystallographic directions with the same accuracy. In the case of thin films, it is thus possible to bring to the fore possible distortions of the unit cell induced by the epitaxial stress. Here, EXAFS measurements will provide the crystallographic parameters in the Fe films, prior and after the structuration, with an accuracy of around 0.01 Å.

The standard approach consists of extracting the contribution of the nearest neighbors from the total signal using Fourier transforms, and to fit this contribution using the classical EXAFS formula. This procedure can be applied for the analysis of data recorded on bcc systems, where the first and second nearest-neighbors shells are very close (respectively, eight neighbors at 2.486 Å and six neighbors at 2.866 Å). However, the characteristics of the two shells have to be determined by a unique fit of their total contribution involving at least five floating parameters. The patterned Fe films are supposed to be in a distorted bcc structure, where each Fe atom has four close shells of nearest neighbors [see Fig. 2(b)]. A fit of this total contribution would therefore require even more parameters.

On the other hand, the phase derivative (PD) method proposed by Martens *et al.*[22] is very sensitive to relative positions of different neighbor shells but does not allow us to extract the width of the radial distribution functions (RDF). As we are interested in a precise determination of the relative position of the different shells, we adopt the PD method. It will provide a clear evidence of the structural relaxation occurring in the patterned film. Furthermore, comparisons between experimental data recorded for three x-ray incident angles (with the linear polarization either parallel or perpendicular to the Fe film plane) and theoretical simulations allow us to determine the crystallographic parameters of the Fe layer before and after the AS process. In a second step, we will check that the extracted distances give correct simulations of the nearest-neighbor signal with RDF's width as floating parameters.

B. Experimental procedure

The experiments were carried out at the Laboratoire pour l'Utilisation du Rayonnement Electromagnétique (LURE France), on the wiggler beam line of the DCI storage ring, using a Ge(220) double-crystal monochromator, at the Fe *K* edge (7110 eV). The spectra were recorded in the fluorescence yield mode, with the samples cooled at 77 K, in order to improve the accuracy of the crystallographic study. As pointed out above, both for continuous and patterned films, different absorption spectra have been recorded in order to measure the lattice distortion: in normal incidence (NI—linear polarization of the x ray parallel to the film plane and either parallel or perpendicular to the Fe stripes) and in grazing incidence (GI—linear polarization of the x ray at about 75° from the film plane).

C. Polarization dependence of the nearest-neighbors shell EXAFS signal

In Fig. 3(a) we present the absorption spectra recorded on the continuous 50-Å Fe film (CF) in NI and GI. The bulk bcc iron spectrum is also shown. In Fig. 3(b) are plotted the absorption spectra recorded on the patterned film in GI and in the two different NI's with the polarization direction parallel (PA) and perpendicular (PE) to the Fe stripes. The EXAFS oscillations were extracted using the classical procedure. A Fourier transform (FT) of the EXAFS oscillations [see Figs. 4(a) and (b)], gives a series of peaks corresponding to the different shells of neighbors of the excited Fe atom. The back FT of the first peak allows to isolate the contribution of the nearest neighbors from the total EXAFS signal.

In the simplest case, where these nearest-neighbors shell only includes N_1 neighbors of the same chemical species at a unique distance R_1, the contribution to the EXAFS signal of this shell can be simply written as[28,29]

$$\chi_1(k)=\frac{N_1^*}{k\cdot R_1^2}B(k)e^{-2k^2\sigma^2}\sin[2kR_1+\varphi(k)];$$

χ_1 is a function of k, the wave vector of the photoelectron created in the absorption process, which is related to the photon energy $\hbar\omega$. $B(k)$ (Fe backscattering amplitude) and $\varphi(k)$ (phase shift) are electronic parameters. σ is the mean square relative displacement, giving the width of the radial distribution function. σ contains two contributions: the thermal agitation (Debye-Waller factor) and the static disorder. N_1^* is an apparent number of first nearest neighbors, given by

$$N_1^*=3\sum_{j=1}^{N_1}\cos^2\alpha_j, \tag{1}$$

where α_i is the angle between the polarization of the x rays and the bond between a Fe atom and his jth atom of the first nearest-neighbor shell. From this formula, valid only for *K* edges, it appears that the EXAFS oscillations depend on the polarization direction of the x rays with respect to the sample crystallographic structure: the contribution of each bond to the total signal is weighted by a the cosine to the square of the angle between the bond and the polarization of the light. Thus the weight of a precise type of bond can be enhanced or

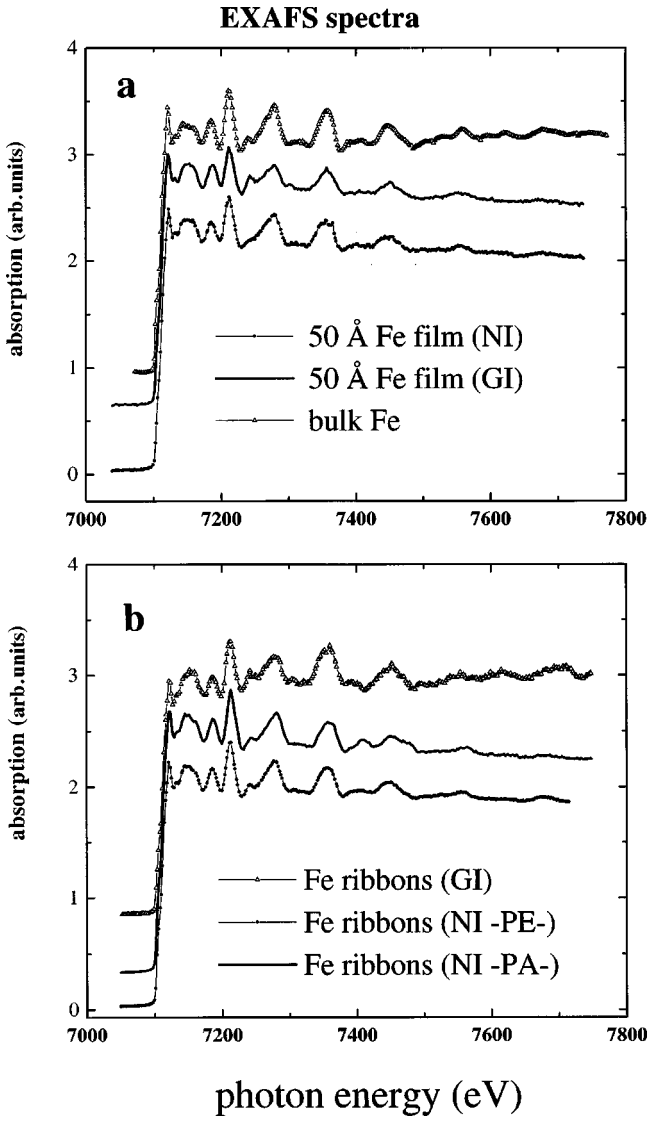

FIG. 3. (a) EXAFS raw spectra recorded on the as-deposited 50-Å Fe film for the two x-ray angles of incidence (NI and GI). The bulk Fe EXAFS spectrum is also reported. (b) EXAFS raw spectra recorded on the patterned 50-Å Fe film for the three x-ray angles of incidence.

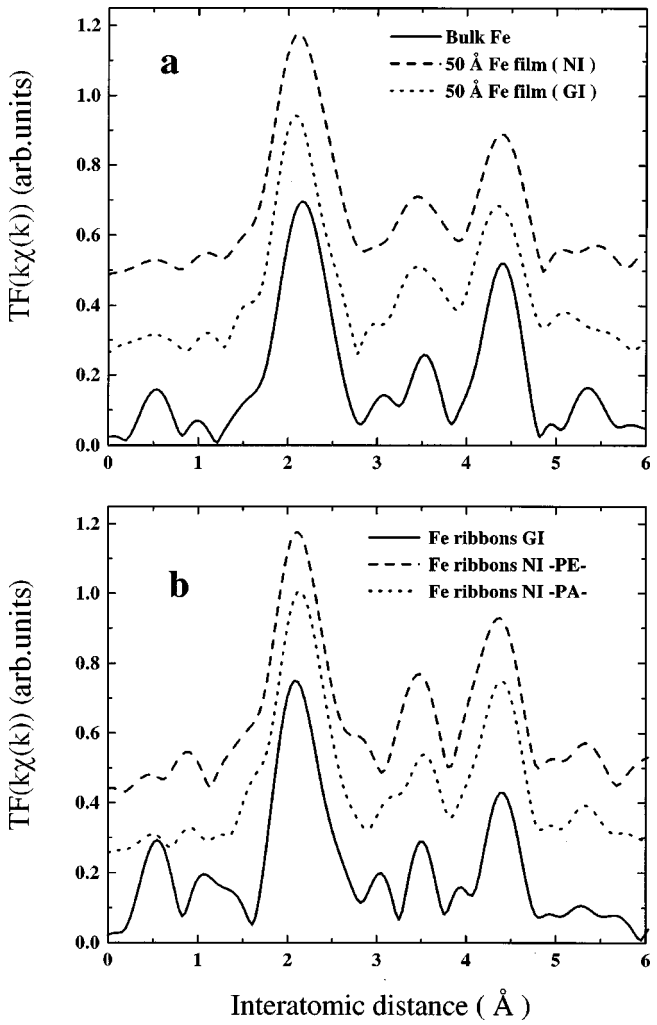

FIG. 4. (a) Fourier transforms (FT) of the EXAFS spectra recorded on the as-deposited 50-Å film and on the bulk Fe film. The FT is performed with a [1.3–2.9 $Å^{-1}$] k window. (b) Fourier transforms (FT) of the EXAFS spectra recorded on the patterned 50-Å film. The FT is performed with the [1.3–2.9 $Å^{-1}$] k window.

canceled, by changing the angle between the incident x rays and the crystallographic axis of the sample.

1. Continuous film

In the as-deposited films, the Fe bcc structure is supposed to be laterally stretched by the epitaxy on the MgO substrate. This lateral expansion should induce a longitudinal compression of the cubic unit cell, leading to a body-centered-tetragonal structure, with lattice parameters a and c. In this structure, presented in Figs. 2(a) and (b) the first neighbor shell, located at $(\sqrt{3}/2)a$ in the case of Fe bulk, is now at $R_1=\frac{1}{2}\sqrt{c^2+2a^2}$. Each Fe atom has four neighbors located at $R_3=a$ in the same (001) plane, two neighbors on an axis perpendicular to the film plane located at a distance $R_2=c$.

For this sample, we have recorded two absorption spectra, with the x rays coming in NI and GI. A simple calculation using formula (1) shows that, in NI, the neighbors located at R_2 do not contribute to the EXAFS signal, whereas the four neighbors located at R_3 have an apparent weight of 6, the eight neighbors at R_1 having an apparent weight of around 8, depending on the cubic cell tetragonalization. In GI, the neighbors located at R_3 do not contribute to the EXAFS signal, whereas the four neighbors located at R_2 have an apparent weight of 6, the eight neighbors at R_1 having an apparent weight of about 8. For this distorted bcc structure, whatever is the x ray angle of incidence, R_1, R_2, and R_3 being very closed distances, there will be always two types of neighbors contributing to the nearest-neighbors EXAFS signal.

2. Patterned film

In the patterned film, the structure is expected to be monoclinic and described by three crystallographic parameters α', β' (in-plane half diagonals), and c' [Figs. 2(c) and (d)]. In this structure, the shell constituted by the eight atoms at $R_1=\frac{1}{2}\sqrt{c^2+2a^2}$ in the stretched bcc structure is now split into two shells of four atoms located at distances $R_1'=\sqrt{c'^2/4+\alpha'^2}$ and $R_1''=\sqrt{c'^2/4+\beta'^2}$. Concerning the second neighbor shell, each Fe atom has four neighbors located

at $R_3'=a'=\sqrt{\alpha'^2+\beta'^2}$ in the same (001) plane and two neighbors on an axis perpendicular to the film plane located at a distance $R_2'=c$.

On the patterned film, we have recorded three absorption spectra. A GI spectrum, with the linear polarization of the x rays perpendicular to the film plane, and two NI spectra, with the linear polarization of the x rays parallel to the film plane, but either parallel or perpendicular to the ribbons. One can once again estimate the apparent weight of each type of bond using formula (1). In GI, the neighbors located at R_3' do not contribute to the EXAFS signal; the nearest-neighbors contribution will be a mixing of the three other shells contributions. In NI, with the polarization vector along the stripes, the neighbors located at R_2' and R_1'' do not contribute to the EXAFS signal; the contribution of the nearest-neighbors shell will be due to the R_3' and R_1'' shells. On the other hand, in NI, but with the polarization vector perpendicular to the stripes, only the neighbors located at R_3' and R_1'' contribute to the EXAFS signal. For this distorted bcc structure, whatever is the x-ray angle of incidence, the nearest-neighbor contribution to the EXAFS signal involves two or three different close shells.

D. Phase derivative method

1. Principle

For both continuous and patterned films, the nearest neighbors is a mixing of contributions from different shells i of Fe neighbors located at very close distances R_i. The classical analysis would consist in fitting this nearest-neighbors signal by the theoretical EXAFS formula, which can be written as a sum over the i nearest neighbors (of the same chemical species):

$$\chi_{\mathrm{NN}}(k)=\sum_i \frac{N_i^*}{k\cdot R_i^2}B(k)e^{-2k^2\sigma_i^2}\sin[2kR_i+\varphi(k)]. \quad (2)$$

As discussed above, we adopt the phase derivative (PD) analysis. The difference between two interatomic distances can be determined by considering the total phase of $\chi_{\mathrm{NN}}(k)$. This differential method is very well suited for the measurement of lattice deformations, as shown by D. T. Jiang, Crozier, and Heinrich.[30] In the simplest case where $\chi_{\mathrm{NN}}(k)$ implies only two types of neighbors, located at distances R_1 and R_2, the total phase can be easily calculated. We first write $\chi_{\mathrm{NN}}(k)$ as

$$\chi_{\mathrm{NN}}(k)=+\mathrm{Im}\left(\frac{A_1(k)}{k}\exp i[2kR_1+\varphi(k)]+\frac{A_2(k)}{k}\exp i[2kR_2+\varphi(k)]\right)$$

$$\text{with}\quad A_i(k)=\frac{N_i^*}{R_i^2}B(k)\exp^{-2k^2\sigma_i^2}$$

so that finally

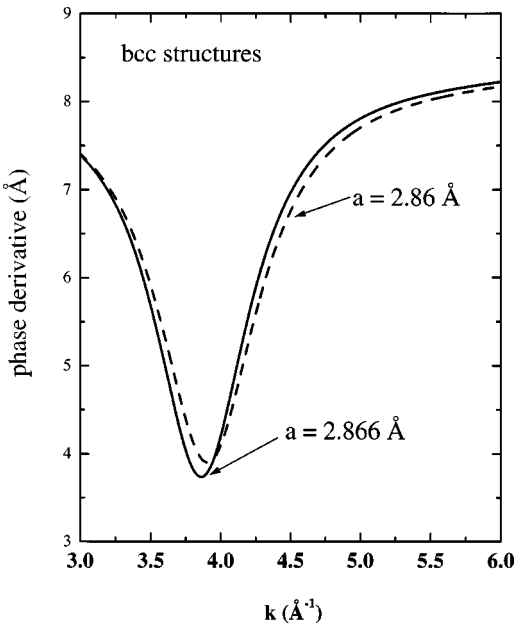

FIG. 5. Phase derivatives (PD) of the experimental χ_{NN} signal obtained from the bulk Fe EXAFS spectrum. Phase derivatives simulations done with the FEFF code considering two different bcc cells are also plotted (a)=2.866 Å, (a)=2.86 Å.

$$\chi_{\mathrm{NN}}(k)=\mathrm{Im}\left[\left(\frac{A_1(k)}{k}\exp(-2ik\Delta R)+\frac{A_2(k)}{k}\exp(2ik\Delta R)\right)\exp[ik(R_1+R_2)+\varphi(k)]\right]$$

or

$$\chi_{\mathrm{NN}}(k)=\frac{\tilde{A}(k)}{k}\sin[2k\tilde{R}+\tilde{\varphi}(k)],$$

where

$$\tilde{A}(k)=A_1(k)\sqrt{1+\left(\frac{A_2(k)}{A_1(k)}\right)^2+2\frac{A_2(k)}{A_1(k)}\cos(k\Delta R)},$$

$$\tilde{\varphi}(k)=\varphi(k)+\tan^{-1}\left(-\frac{A_1(k)-A_2(k)}{A_1(k)+A_2(k)}\tan(k\Delta R)\right),$$

$$\tilde{R}=\frac{R_1+R_2}{2}\ \text{ and }\ \Delta R=R_2-R_1;$$

$\tilde{\varphi}(k)$ is the $\chi_{\mathrm{NN}}(k)$ total phase. Under some assumptions (which will be detailed later), one can show that kinks occur in this total $\tilde{\varphi}(k)$ for some k values linked to the ΔR value by[22]

$$k_{2n+1}\approx\frac{(2n+1)\pi}{2\Delta R}. \quad (3)$$

As we shall see, the kink position is located by taking the derivative of the total phase with respect to k. The example of bulk bcc Fe is given in Fig. 5. We have extracted the nearest-neighbors contribution from the experimental EXAFS spectrum and calculated the associated phase derivative. It is compared with a theoretical calculation done with

the FEFF code[31] on bulk Fe with a lattice parameter $a=2.866\,\text{Å}$ (first neighbors at 2.482 Å and second neighbors at 2.866 Å, $\Delta R=0.384\,\text{Å}$). The general shape of the experimental phase derivative and its minimum at $k_{\min}=3.86\,\text{Å}^{-1}$ are very well reproduced by the FEFF simulation. Let us point out that the phase derivative calculated for a slightly different bcc structure ($a=2.86\,\text{Å}$, $\Delta R=0.383\,\text{Å}$) shows a minimum at a significantly different k position ($k_{\min}=3.91\,\text{Å}^{-1}$). This demonstrates the width precision of the method for the determination of the ΔR value. We will use the same procedure to analyze the structure of the as-deposited and patterned Fe films: the experimental phase derivative will be compared to simulations calculated for distorted bcc structures. The simulated phase derivatives will be simultaneously fit to the data recorded for the different x-ray incident angles. This way, despite supposed complex Fe structures, the number of adjusted parameters will not exceed 3.

2. Simple formulation

Of course, the analysis would be much easier if one could extract directly ΔR from the k-position value of the phase minimum using a simplified expression of formula (3). One can first assume that the phase shift $\varphi(k)$ contained in the total phase $\tilde{\varphi}(k)$ varies linearly with k.[32] A second approximation consists in assuming that $\sigma_1^2=\sigma_2^2$ (i.e., the two shells of neighbors have the same radial distribution width). In this case, the ratio

$$C=\frac{A_1(k)-A_2(k)}{A_1(k)+A_2(k)}$$

does not depend on k anymore. Thus, with these two approximations, one can easily calculate the second derivative of the total phase $\tilde{\varphi}(k)$:

$$\frac{d^2\tilde{\varphi}}{dk^2}\approx\frac{-4C(k)(\Delta R)^2\sin(2k\Delta R)}{\left(1-C(k)+\dfrac{4C(k)}{1+C(k)}\cos^2(k\Delta R)\right)^2}.$$

From this formula, it appears clearly that the total phase first derivative shows a minimum at

$$k_{\min}=\frac{\pi}{2\Delta R}. \tag{4}$$

The analysis of the beating position can therefore allow to determine quantitatively ΔR.

We have checked this simple relation and the validity of our assumptions on bulk bcc iron. As indicated above, the bond-length difference between the two shells involved in the nearest-neighbor signal is $\Delta R=0.38\,\text{Å}$. The minimum of the experimental phase derivative is at $k_{\min}^{\exp}=3.86\,\text{Å}^{1}$. This value is quite different from the theoretical one obtained using Eq. (4) $k_{\min}^{\text{theo}}=4.085\,\text{Å}^{-1}$. The difference is due to the assumptions we made on the k dependence of $\varphi(k)$ and $[A_1(k)-A_2(k)]/[A_1(k)+A_2(k)]$.

We have considered simulations done with the FEFF 6.0 code using phase shifts and backscattering amplitudes calculated by the code. The results were already shown to be very satisfactory for $3d$ transition metals.[33] Simulations were done on many structures that one expects to be close to the studied ones (bcc structures slightly distorted along several crystallographic directions). For all these structures, we have plotted ΔR as a function of $k_{\min}$. We have shown that one can write

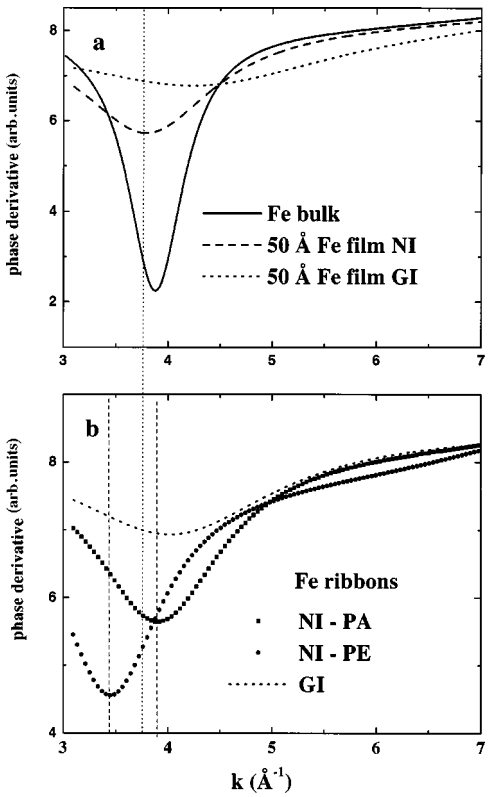

FIG. 6. (a) Phase derivatives (PD) of $\chi_{\text{NN}}(k)$ extracted from experimental data recorded on the as-deposited 50-Å Fe film for the two different x-ray incident angles (NI and GI). One can observe that the minima of the two PD signals are located to distinct positions. (b) Phase derivatives (PD) of $\chi_{\text{NN}}(k)$ extracted from experimental data recorded on the patterned 50-Å Fe film for the three distinct directions of x-ray incidence. In NI, one can observe that the minimum of the PD corresponding to the as-deposited film [pointed out by the short dotted line (a)] is split up into two different minima after the structuration process (pointed out by dashed lines) depending on the polarization direction (perpendicular PE or parallel PA to the ribbons).

$$\Delta R=\frac{\pi}{2(k_{\min}+\langle\Delta K\rangle)}\pm 0.01\,\text{Å}, \tag{5}$$

where $\langle\Delta k\rangle=0.21\,\text{Å}^{-1}$ stands for a correction to the formula (4) and depends on the used FT window. The 0.01-Å error comes from the dispersion of the different points around this mean straight line.

The structures that we shall study are rather close to the bulk bcc iron structure to assume that this formula remains valid in all cases for each x-ray polarization direction. So, the use of this phenomenological relation can provide an approximate value of ΔR, which can be used as a starting point before a refinement of the model using the FEFF code.

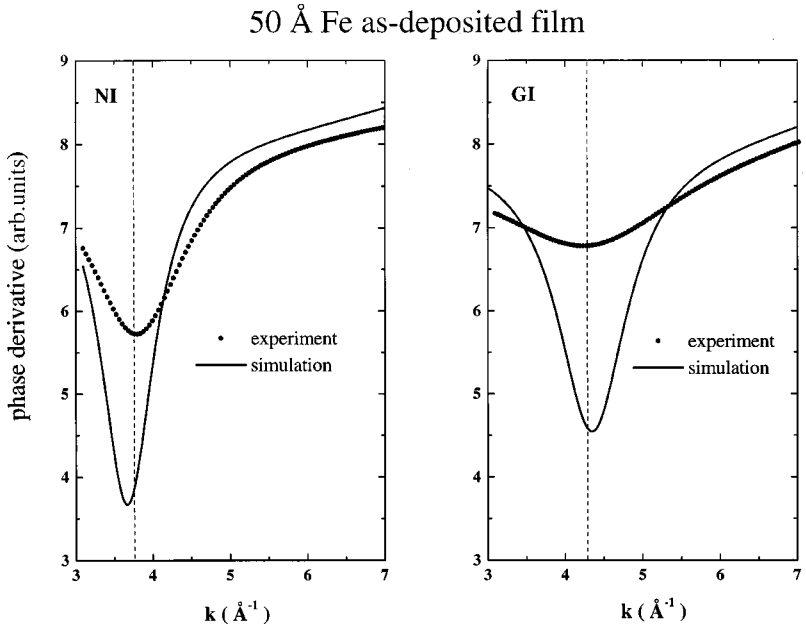

FIG. 7. Simulations of the phase derivatives (PD) signal done with the FEFF code concerning the as-deposited 50-Å Fe film. The minima of the PD signal are adjusted simultaneously for the two directions of x-ray incidence. The best agreement is found for a bct structure given by the two parameters $a=2.82$ Å and $c=2.92$ Å.

E. Data analysis

1. Continuous 50-Å Fe film (CF)

In Fig. 6(a), we report the total phase derivative with respect to k, $(d\tilde{\varphi}/dk)$, for the two x-ray incident angles recorded on the continuous 50-Å Fe film (CF). The bulk bcc Fe experimental phase derivative is also reported, with its minimum at 3.86 Å^{-1} corresponding to $\Delta R=0.384$ Å. For the CF, we clearly observe that the minimum is located at different positions for the NI and GI spectra. This nonisotropic result demonstrates that iron is not in a cubic structure. Due to the lattice mismatch between the MgO substrate and bulk Fe, we have assumed (Sec. IV C) a tetragonal crystallographic structure of the Fe CF resulting from a laterally stretched bcc structure. In this case, the beating position in NN signal total phase should be at a lower k value in NI. As a matter of fact, in NI (respectively GI), the two neighbor shells contributing to the signal are located at R_1 and R_3 (respectively, R_1 and R_2). This corresponds to $\Delta R^{\mathrm{NI}} > \Delta R^{\mathrm{GI}}$, and therefore $k_{\min}^{\mathrm{NI}} < k_{\min}^{\mathrm{GI}}$ according to formula (5), as it is experimentally observed. The bond-length difference between the two neighbor shells concerned in GI ($\Delta R^{\mathrm{GI}} = R_2 - R_1$) is shorter than the one measured in NI ($\Delta R^{\mathrm{NI}} = R_3 - R_1$). Fe appears to be in bct structure, expanded in the interface plane and compressed along the growing direction by comparison to the bulk bcc Fe cell.

From the knowledge of the two bondlength differences ΔR, we can in principle accede to the approximate values of R_2 and R_3 (i.e., the two crystallographic parameters a and c). Nevertheless, one must be aware that an error of 0.01 Å on ΔR can lead to an error on the a or c parameters close to 0.1 Å. This shows that using formula (5) one needs to keep a differential relation. From formula (5), the difference $(a-c)$ easily writes

$$a-c=R_3-R_2=\frac{\pi}{2}\left(\frac{1}{k_{\min}^{\mathrm{NI}}+\langle\Delta k\rangle}-\frac{1}{k_{\min}^{\mathrm{GI}}+\langle\Delta k\rangle}\right).$$

The experimental values $k_{\min}^{\mathrm{NI}}=3.72$ Å^{-1} and $k_{\min}^{\mathrm{GI}}=4.42$ Å^{-1} leads to $\Delta R^{\mathrm{NI}}\approx 0.40\pm 0.01$ Å and $\Delta R^{\mathrm{GI}}\approx 0.33\pm 0.01$ Å which gives $a-c\approx 0.07\pm 0.02$ Å.

Starting from this relation, the analysis consists now in optimizing the bct cell in order to adjust the minima of the phase derivative calculated with the FEFF code to the experimental ones for each x-ray incident angle. This procedure has been done by successive 0.01 Å steps for the two parameters a and c. The results are reported in Fig. 7. We obtain a good agreement with the experimental data for $a=2.92$ Å and $c=2.82$ Å. One can notice that the location of the phase derivative minima can be conveniently adjusted, whereas the signal general shape is not perfectly reproduced. We will discuss this point in the next section.

We have checked that the NN contribution can be fitted in a satisfactory way with the classical EXAFS formula (2) using the crystallographic parameters close to the ones determined above. The results are shown in Fig. 8. The best agreement is found for $R_1=2.495$ Å, $R_3=2.91$ Å, and $R_2=2.82$ Å, values very close to the ones derived from the previous method. The combination of these analyses gives therefore $a=2.915\pm 0.015$ Å and $c=2.82\pm 0.01$ Å as crystallographic parameters for the Fe/MgO as-deposited film. These results are in accordance with the work performed by O. Durand *et al.*[23] on thicker 800-Å Fe films. Their studies show a residual 0.6% compressive strain along the surface normal of the film.

2. Patterned Fe film (PF)

Figure 4(b) compares the FT of the EXAFS signal recorded on the patterned film (PF) for different x-ray polarization directions. In NI, for the polarization perpendicular to stripes (PE), the nearest-neighbor peak is located at a slightly lower R position than the peak obtained for the polarization parallel to the stripes (PA). This shows that the mean NN bond length must be shorter along the PE crystallographic

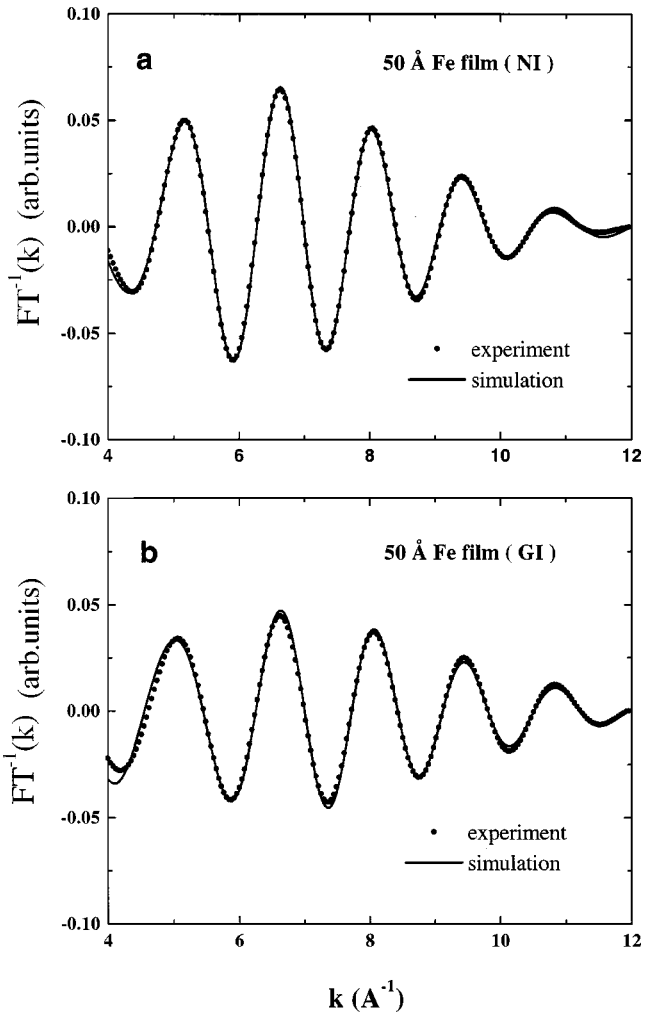

FIG. 8. Results of simulations done on the nearest neighbors $\chi_{NN}(k)$ contribution of the EXAFS signal concerning the as-deposited 50-Å Fe film for the two different directions of x-ray incidence [NI (a) and GI (b)]. The best agreement is found for a bct structure given by the two parameters $c=2.82$ Å and $a=2.91$ Å ($\alpha=\beta=2.07$ Å).

axis than in the PA direction. Here also, the PD analysis will allow us to determine the different crystalline parameters. Figure 6(b) displays the phase derivatives extracted from experimental data recorded on the patterned film for the three polarization directions, compared to the one obtained on the CF [Fig. 6(a)]. The two NI spectra measured on the PF present minima located at different k values exhibiting a non-square symmetry in the planes parallel to the interface.

According to our notations, the bond-length difference of the two first shells along the specific crystallographic direction writes

$$\Delta R_{\mathrm{PE}}^{\mathrm{NI}}=R_3'-R_1'',$$

$$\Delta R_{\mathrm{PA}}^{\mathrm{NI}}=R_3'-R_1',$$

$$\Delta R^{\mathrm{GI}}\approx R_2'-\tfrac{1}{2}(R_1'+R_1'').$$

In principle, all the crystallographic parameters (α', β', and c') can be deduced from these three ΔR values. In practice, as previously described, one can only extract the bond-length difference:

$$\Delta R_{\mathrm{PE}}^{NI}-\Delta R_{\mathrm{PA}}^{\mathrm{NI}}=R_1'-R_1''=\sqrt{\left(\frac{c'}{2}\right)^2+\alpha'^2}-\sqrt{\left(\frac{c'}{2}\right)^2+\beta'^2}$$

$$=\frac{\pi}{2}\left(\frac{1}{k_{\min}^{\mathrm{PE}}+\langle\Delta k\rangle}-\frac{1}{k_{\min}^{\mathrm{PA}}+\langle\Delta k\rangle}\right),$$

α' and β' being close to the corresponding value of bulk Fe ($\alpha=\beta=a/\sqrt{2}\approx 2.03$ Å), one can easily show that

$$\sqrt{\frac{2}{3}}(\alpha'-\beta')=\frac{\pi}{2}\left(\frac{1}{k_{\min}^{\mathrm{PE}}+\langle\Delta k\rangle}-\frac{1}{k_{\min}^{\mathrm{PA}}+\langle\Delta k\rangle}\right).$$

Using this approximate relation and the experimental values $k_{\min}^{\mathrm{PE}}=3.43$ Å^{-1} and $k_{\min}^{\mathrm{PE}}=3.90$ Å^{-1}, we obtain $\alpha'-\beta'=0.06$ Å. As we did in the case of the CF, starting from this result, the method consists in optimizing the crystalline structure defined by α', β', and c' in order to fit the experimental minimum positions of the phase derivative with the ones calculated with the FEFF code for the three polarization directions. It has been done by varying all the parameters by steps of 0.005 Å. Results are reported in Fig. 9.

The best agreement is obtained for $\alpha'=2.07$ Å, $\beta'=2.02$ Å, and $c'=2.83$ Å with a precision of about 0.01 Å.

3. Effects of disorder

As for the CF, the general shape of the experimental phase derivative is not well reproduced by the FEFF code. Indeed, our calculations do not take into account the radial dispersion of interatomic distances. We have checked that the curvature of the phase derivative can be linked to the width of the RDF. This was done by modifying artificially the Debye temperature in the FEFF input file. Increasing the width of the RDF leads to flatter phase derivatives keeping unchanged the position of the minimum. The flat experimental phase derivative obtained in GI tends to prove that the c' parameter value is largely distributed around its mean value along the surface normal.

Following the classical method, χ_{NN} functions have been fitted using formula (2) taking R_1', R_2', R_3', and R_3'', as free parameters. The best agreement (Fig. 10) is found for $R_1'=2.89$ Å, $R_2'=2.84$ Å, $R_3'=2.51$ Å, and $R_3''=2.47$ Å corresponding to $\alpha'=2.07$ Å, $\beta'=2.02$ Å, and $c'=2.84$ Å which is consistent with the phase derivative analysis.

As a conclusion, in both CF and PF cases, we have shown that the phase derivative analysis of the x-ray-absorption spectra allow us to determine precisely any bcc-like crystallographic structure by using simulations calculated by the FEFF code. Even if the local disorder can hardly be taking into account in the FEFF simulations, we have demonstrated that it affects neither the location of the phase derivative minimum, nor the precision in the determination of ΔR.

VI. DISCUSSION—ELASTIC MODELS

Let us first consider the CF case. By comparison to the bulk bcc Fe structure, the bct cell of the CF ($c/a\approx 1.033$) is

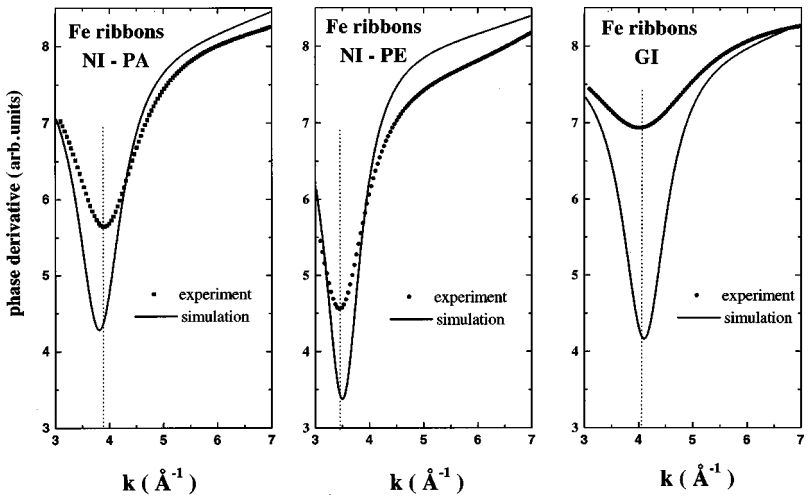

FIG. 9. Simulations of the phase derivatives (PD) signal done with the FEFF code concerning the patterned 50-Å Fe film. The minima of the PD signal are adjusted simultaneously for the three distinct directions of x-ray incidence. The best agreement is found for a distorted bct structure given by the three parameters $c'=2.83$ Å, $\alpha'=2.07$ Å, and $\beta'=2.02$ Å.

then $1.9\pm0.6\%$ expanded in the plane and $-1.6\pm0.6\%$ compressed along the surface normal. The epitaxial relationship between Fe and MgO (mismatch close to $+4\%$) induces an isotropic expansion of the Fe cell along the two in-plane directions, coupled with a compression of the cell along the surface normal as predicted by the elastic model:

$$\varepsilon_{\perp}=-\frac{2C_{12}}{C_{11}}\varepsilon_{\parallel}\approx-\varepsilon_{\parallel};$$

C_{11} and C_{12} are elastic constants.

The quite flat profile of the phase derivative recorded in GI is connected to a large radial distribution of the c parameter around its mean value. This distribution is certainly imposed by the strain relaxation occurring in the film volume, as indicated by the ''stand-off'' dislocations observed by HRTEM. In the EXAFS signal, each Fe layer contributes with the same weight. The 1.9% mean dilatation appears to be an average value on the whole film thickness. This measurement does not exclude a 3.8% expansion of the Fe lattice at the interface Fe-MgO and a strain relief in the volume of the film.

The case of the patterned film is very interesting. EXAFS experiments have provided a clear proof of a uniaxial relaxation of the crystalline parameter along the PE direction. Indeed, β parameter is lowered from 2.07 to 2.02 Å ($\beta_{\text{bulk}}=2.03$ Å) after the structuration process whereas the equivalent parameter along the PA direction equal to 2.07 Å remains unchanged. This leads to an uniaxial relief δ of the strain field along the direction perpendicular to the step edges equal to $\delta=(\beta'-\alpha')/\alpha'=-2.5\pm0.6\%$. In addition, after process, the value of the c' parameter along the growing axis increases from 2.82 ± 0.01 Å to 2.835 ± 0.015 Å leading to an out-of-plane strain relief $\Delta\varepsilon_{\perp}=(c'-c)/c\approx+0.5\%$.

According to the elastic model, in-plane and out-of-plane strain relaxation must be linked by the following relation:

$$\Delta\varepsilon_{\perp}=-\frac{C_{12}}{C_{11}}\Delta\varepsilon_{\parallel}=-\frac{C_{12}}{C_{11}}\delta\approx-0.6\delta.$$

This relation is not exactly satisfied in our case, certainly because of the large dispersion of the c and c' parameters evidenced by the shape of the PD. However, the variation of the relaxation measured in the surface normal direction is coherent with the elastic theory predictions: an in-plane compression of the cell must be associated with an out-of-plane dilatation, as found by EXAFS experiments.

Moreover, it appears very interesting to compare the component of the stress along the PE direction σ_{PE} before and after the AS process. The elastic model gives the generic relation (we assume a material with isotropic mechanical properties)

$$\sigma_{\text{PE}}=C_{11}\varepsilon_{\text{PE}}+C_{12}(\varepsilon_{\text{PA}}+\varepsilon_{\perp}).$$

Thus we have

$$\frac{\sigma_{\text{PE}}(\text{CF})-\sigma_{\text{PE}}(\text{PF})}{\sigma_{\text{PE}}(\text{CF})}=\frac{-\left(\delta+\dfrac{C_{12}}{C_{11}}\Delta\varepsilon_{\perp}\right)}{\left(1+\dfrac{C_{12}}{C_{11}}\right)\varepsilon_{\parallel}+\dfrac{C_{12}}{C_{11}}\varepsilon_{\perp}}\approx1$$

which gives $\sigma_{\text{PE}}=0$ in the case of the PF. This means that the main feature of the AS process is to release the stress along the peculiar direction perpendicular to the step edges.

From this precise crystallographic characterization, we will now show that it is possible to explain the magnetic properties observed in the patterned film via a simple magnetoelastic model.

VII. MAGNETOELASTIC MODEL

The magnetoelastic energy associated to an in-plane relaxation of the elastic strain field in the PF writes[34]

$$E_{m-e}=B_1(\varepsilon'_{11}\alpha'^2_1+\varepsilon'_{22}\alpha'^2_2)+2B_2\varepsilon'_{12}\alpha'_1\alpha'_2,$$

where B_i are the magnetoelastic coefficients, ε'_{ij} is the strain tensor and α'_i coordinates of the unitary magnetization vector expressed in the standard Fe [100] basis. For convenience, one can write this formula in the basis rotated by 45°

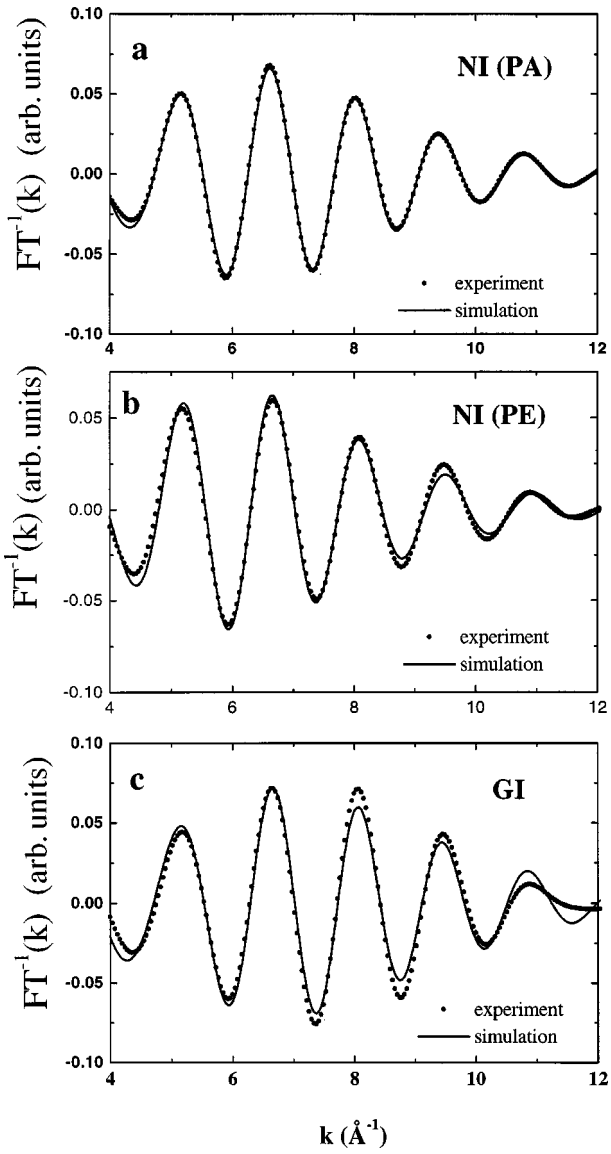

FIG. 10. Results of simulations done on the nearest neighbors $\chi_{NN}(k)$ contribution of the EXAFS signal concerning the patterned 50-Å Fe film for the three different directions of x-ray incidence [NI (a) and GI (b)]. The best agreement is found for a distorted bct structure given by the three parameters $c'=2.84$ Å, $\alpha'=2.07$ Å, and $\beta'=2.02$ Å.

in the plane of the film, i.e., linked to the stripes. In this new [PE, PA] basis, let us call ε_{ij} the strain tensor components and α_i the magnetization vector coordinates.

$$E_{m-e}=B_1\left(\frac{\varepsilon_{PE}+\varepsilon_{PA}}{2}\right)+2B_1\varepsilon_{12}\alpha_{PA}\alpha_{PE}$$

$$+\frac{B_2}{2}(\varepsilon_{PE}-\varepsilon_{PA})(\alpha_{PE}^2-\alpha_{PA}^2).$$

The uniaxial strain relaxation along the PE Fe direction evidenced by the EXAFS measurement can be expressed as $\delta=\varepsilon_{PE}$ that yields to

$$E_{m-e}=\frac{B_2\delta}{2}(\alpha_{PE}^2-\alpha_{PA}^2).$$

Then, the energy difference between the two respective magnetization orientations, perpendicular ($\alpha_{PE}=1$) and parallel ($\alpha_{PA}=1$) to the ribbons writes

$$\Delta E_{m-e}=B_2\delta\sim-1.9\times10^6\ \text{erg/cm}^3<0$$

(with $B_2=7.62\times10^7$ erg/cm^3) (Ref. 35).
The magnetoelastic energy is minimum when the magnetization is oriented perpendicularly to the stripes as observed in the magneto-optical measurements. The anisotropy field H_S given by $H_S=2\Delta E/M_S$ is roughly equal to 2250 Oe, very close to one determined experimentally (2400 Oe) which proves the validity of this simple magnetoelastic model.

VIII. CONCLUSION

We have presented a detailed structural EXAFS study of thin Fe films grown on MgO(001) substrate. The crystallographic structure of the as-deposited film is clearly seen to be body-centered tetragonal because of the interfacial strain due to the epitaxy. The result is that the Fe unit cell is expanded in the plane and compressed along the growth axis as compared to the bulk bcc Fe cell. EXAFS experiments were also carried out on a 50-Å-thin Fe film patterned into ribbons by the AS method and characterized by a strong uniaxial magnetic anisotropy with the easy axis lying along the perpendicular to the ribbons. We have clearly shown that this magnetic anisotropy is correlated to a relaxation of the elastic strain field occurring perpendicularly to the ribbons in the magnetic film, leading to a slightly distorted bct cell. Magnetoelastic effects are then demonstrated to be directly at the source of the magnetic anisotropy. This work has provided clear evidence of the relation between structure and magnetism.

*Author to whom correspondence should be addressed: Laboratoire Central de Recherches CNRS-Thomson, Unité Mixte de Physique, Domaine de Corbeville, 91404 Orsay Cedex 4, France. Electronic address: jaffres@lcr.thomson-csf.com

[1] J. G. Gay and R. Richter, Phys. Rev. Lett. **56**, 2728 (1986).
[2] R. Allenspach, M. Stampanoni, and A. Bishof, Phys. Rev. Lett. **65**, 3344 (1990).
[3] J. Pommier, P. Meyer, G. Penissard, P. Bruno, J. Ferré, and D. Renard, Phys. Rev. Lett. **65**, 2054 (1990).
[4] T. Kingetsu and K. Sakai, Phys. Rev. B **48**, 4140 (1993).
[5] C. Chappert and P. Bruno, J. Appl. Phys. **64**, 5736 (1988).
[6] N. Marsot, R. Belkhou, H. Magnan, P. Le Fèvre, C. Guillot, and D. Chandesris, Phys. Rev. B **59**, 3135 (1999).
[7] F. Nguyen Van Dau, M. Sussiau, A. Schuhl, and P. Galtier, J. Appl. Phys. **81**, 1 (1997).
[8] M. Sussiau, F. Nguyen Van Dau, P. Galtier, A. Encinas, and A. Schuhl, J. Magn. Magn. Mater. **165**, 1 (1997).
[9] J. Chen and J. L. Erskine, Phys. Rev. Lett. **68**, 1212 (1992).
[10] D. J. Huang, J. Lee, G. A. Hulhollan, and J. L. Erskine, J. Appl. Phys. **73**, 6751 (1993).
[11] P. Krams, B. Hillebrands, G. Güntherodt, and H. P. Oepen, Phys. Rev. B **49**, 3633 (1994).

[12] B. Hillebrands, J. Fassbender, R. Jungblut, G. Güntherodt, D. J. Roberts, and G. A. Gehring, Phys. Rev. B **53**, R10 548 (1996).
[13] R. K. Kawakami, M. O. Bowen, H. J. Choi, E. J. Escorcia-Aparicio, and Z. Q. Qiu, Phys. Rev. B **58**, R5924 (1998).
[14] A. Berger, U. Linke, and H. P. Oepen, Phys. Rev. Lett. **68**, 839 (1992).
[15] H. P. Oepen, C. M. Schneider, D. S. Chuang, C. A. Ballentine, and R. C. O'Handley, J. Appl. Phys. **73**, 6186 (1993).
[16] B. Hillebrands and J. R. Dutcher, Phys. Rev. B **47**, 6126 (1993).
[17] R. K. Kawakami, E. J. Escorcia-Aparicio, and Z. Q. Qiu, Phys. Rev. Lett. **77**, 2570 (1996).
[18] J. P. Peyrade, F. Voillot, M. Goiran, H. Atmany, and A. Rocher, Appl. Phys. Lett. **60**, 2481 (1992).
[19] M. Goiran, C. Guasch, F. Voillot, R. Carles, J. P. Peyrade, E. Bedel, and Munoz-Yague, Europhys. Lett. **23**, 647 (1993).
[20] H. Jaffrès, L. Ressier, K. Postava, A. Schuhl, F. Nguyen Van Dau, M. Goiran, J. P. Redoulès, J. P. Peyrade, and A. R. Fert, J. Magn. Magn. Mater. **184**, 19 (1998).
[21] E. Snoeck, L. Ressier, H. Jaffrès, J. P. Peyrade, and A. Schuhl, J. Cryst. Growth **187**, 245 (1998).
[22] G. Martens, P. Rabe, N. Schwentner, and A. Werner, Phys. Rev. Lett. **39**, 1411 (1977).
[23] O. Durand, J. R. Childress, P. Galtier, R. Bisaro, and A. Schuhl, J. Magn. Magn. Mater. **145**, 111 (1995).
[24] J. R. Childress, R. Kergoat, O. Durand, J. M. George, P. Galtier, J. Miltat, and A. Schuhl, J. Magn. Magn. Mater. **130**, 13 (1994).
[25] H. Jaffrès, L. Ressier, J. P. Peyrade, A. R. Fert, P. Gogol, A. Thiaville, A. Schuhl, and F. Nguyen Van Dau, J. Appl. Phys. **84**, 4375 (1998).
[26] L. Ressier, Ph.D. thesis, INSAT, Toulouse, 1997.
[27] K. Postava, J. F. Bobo, M. D. Ortega, B. Raquet, H. Jaffrès, E. Snoeck, M. Goiran, A. R. Fert, J. P. Redoulès, J. Pistora, and J. C. Ousset, J. Magn. Magn. Mater. **163**, 8 (1996).
[28] D. E. Sayers, E. A. Stem, and F. W. Lytle, Phys. Rev. Lett. **27**, 1204 (1971).
[29] O. Heckmann, H. Magnan, P. Le Fèvre, D. Chandesris, and J. J. Rehr, Surf. Sci. **312**, 62 (1994).
[30] D. T. Jiang, E. D. Crozier, and B. Heinrich, Phys. Rev. B **44**, 6401 (1991).
[31] J. J. Rehr, J. Mustre de Leon, S. I. Zabinski, and R. C. Albers, J. Am. Chem. Soc. **113**, 5135 (1991).
[32] B. K. Teo and P. A. Lee, J. Am. Chem. Soc. **101**, 2815 (1979).
[33] P. Le Fèvre, H. Magnan, and D. Chandesris, Surf. Sci. **352-354**, 923 (1996).
[34] R. Koch, M. Weber, K. Thürmer, and K. H. Rieder, J. Magn. Magn. Mater. **159**, L11 (1996).
[35] P. Bruno, Magnetismus von Festkörpen und Grenzflächen, Ferienkurse des Forschungszentrums, Jülich (KFA, 1993), Chap. 24.